

# Light-based Chromatic Aberration Correction of Ultrafast Electron Microscopes

Marius Constantin Chirita Mihaila,<sup>1,\*</sup> Neli Laštovičková Streshkova,<sup>1,\*</sup> and Martin Kozák<sup>1</sup>

<sup>1</sup>Charles University, Faculty of Mathematics and Physics, Ke Karlovu 3, 121 16 Prague 2

(Dated: January 20, 2025)

We propose and theoretically demonstrate a technique that allows one to compensate for chromatic aberrations of traditional electron lenses in ultrafast electron microscopes. The technique is based on space- and time-dependent phase modulation of a pulsed electron beam using interaction with a shaped pulsed ponderomotive lens. The energy-selective focal distance is reached by combining the electron temporal chirp with the time-dependent size of the effective potential, with which the electrons interact. As a result, chromatic aberration can be reduced by up to a factor of seven. This approach paves the way for advanced transverse and longitudinal wavefront shaping of electrons in free space.

## I. INTRODUCTION

Spatial resolution of imaging using photons or electrons is fundamentally limited by the wavelength of the substance used to carry the information from the sample to the detector. However, reaching the diffraction limit of resolution requires an aberration-free imaging system. The challenge of achieving atomic resolution in low-energy electron microscopy comes mainly from aberrations in electron optics. Especially chromatic aberrations severely deteriorate the imaging performance at low electron energies [1–3].

The foundation for understanding and compensating for these aberrations was laid in 1936 [4, 5]. The Scherzer theorem established that chromatic and spherical aberrations are inevitable in rotationally symmetric electron lenses. This theorem underscored a critical limitation in electron microscopy, setting the stage for decades of research aimed at overcoming these inherent aberrations. In 1947, it was demonstrated that chromatic and spherical aberrations in electron lenses could be theoretically corrected by either removing rotational symmetry, using time-varying fields, or introducing space charges [6].

Later, the correction of spherical aberrations using hexapole correctors was experimentally demonstrated [7, 8]. This breakthrough not only proved the theoretical proposals suggested earlier but also achieved a substantial improvement in resolution, making a significant leap in electron microscopy capabilities.

Ultrafast electron microscopes provide exceptional temporal and spatial resolution [9–11]. Future progress in this field is anticipated through the integration of highly coherent field emission sources [12–14], aberration-corrected probes, and increased probe current.

Although programmable and adaptive optics, such as spatial light modulators (SLM), have revolutionized light optics [15], the development of programmable and adaptive phase plates for electron optics remains in its early stages [16–23]. Recent research has explored the coherent

manipulation of electron waves through interactions with optical near-fields [24–39] and pure optical fields [40–52] in free space. Furthermore, theoretical proposals have shown the correction of spherical aberrations in electron lenses through controlled light interactions [53–56].

We theoretically demonstrate here a method to compensate for chromatic aberrations in traditional electron lenses in ultrafast electron microscopes by pairing their positive chromatic aberrations with a ponderomotive lens exhibiting negative chromatic aberrations. Unlike multipole correctors [3], this method achieves the correction in a single interaction plane, potentially reducing the complexity, spatial requirements, and costs of aberration correctors. Using the interaction between spatially shaped pulsed light and a chirped electron pulse, specifically utilizing the phase shift gradient encountered by the electron pulse at moderate convergence angles of the pulsed optical lens, this approach offers a promising solution to a long-standing challenge in electron microscopy.

## II. THEORETICAL CONSIDERATIONS

The aberration function of electrostatic and magnetostatic electron lenses, which accounts for the chromatic aberration, characterizes the phase shift distortion of the electron wave and can be expressed as [57]:

$$\chi(\alpha, E) \approx \frac{\pi}{\lambda_e(E)} \left[ \Delta z_0 + C_c \frac{E - E_0}{E_0} \right] \alpha^2. \quad (1)$$

with  $\alpha$  the convergence semi-angle, the modified defocus due to the electron energy spread  $\Delta z_0 + C_c \frac{E - E_0}{E_0}$ , where  $C_c$  is the chromatic aberration coefficient and  $\Delta z_0$  is the defocus that can be tuned by the electron lens. Furthermore,  $E_0$  is the mean electron energy and  $E$  is the actual electron energy within the total energy spread  $\Delta E$  of the electron beam. The energy-dependent relativistic electron wavelength is defined as  $\lambda_e(E) = 2\pi\hbar c / (\sqrt{2EE_{r_0} + E^2})$ , with the rest electron energy  $E_{r_0} = m_e c^2$ ,  $\hbar$  the reduced Planck constant,  $m_e$  the electron rest mass, and  $c$  the light velocity in vacuum. For brevity, we denote  $\chi_0 = \chi(\Delta z_0 = 0)$  solely the energy-dependent part of the aberration function.

\* MCCM and NLS with equal contribution. Contact authors : marius.chirita@matfyz.cuni.cz, neli.streshkova@matfyz.cuni.cz

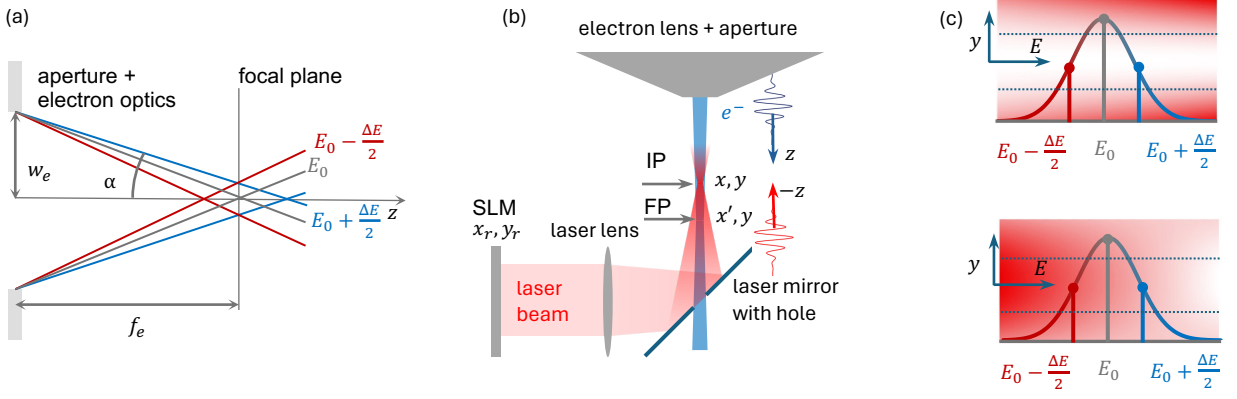


FIG. 1. (a) Electron trajectories with positive chromatic aberration. Due to the energy spread of the electron beam, slower electrons will get focused before the geometric focal plane and faster electrons after. (b) Scheme of the experimental geometry. The optical beam is shaped in front of the SLM plane  $(x_r, y_r)$ , and focused near the interaction plane IP  $(x, y)$  where the chromatic aberration of the electrons is corrected. Subsequently, the electrons are focused in the Fourier plane (FP)  $(x', y')$ . (c) Interaction with a ponderomotive lens generated by a modified vortex beam (top) and a Gaussian beam (bottom). The red color scale illustrates a snapshot of the longitudinal intensity cross-section,  $g^2(y, z)$ . The interaction plane, with a radius of  $< 2 \mu\text{m}$ , where the shaped laser intensity is used for chromatic correction, is shown within the dashed blue lines. Furthermore, a snapshot of the electron beam is represented in its rest frame, where electrons with energy  $E_0 + \Delta E/2$  are placed forward and electrons with energy  $E_0 - \Delta E/2$  are placed backward. The vortex-like beam causes the high energy parts of the electron beam to converge more strongly than the low energy parts. The Gaussian-like beam causes the low energy parts to diverge more strongly than the high energy part. Both induce negative chromatic aberration.

Due to the energy spread of the electrons, faster electrons passing through traditional lenses get focused after the geometrical focal plane, whereas slower electrons focus before it (see Fig. 1(a)).

In the particle picture, when the electrons interact with strong optical fields in vacuum, transverse momentum from the photons is transferred to the electrons, influencing their trajectory. The electrons are repelled from areas with high photon density [58]. A suitably shaped optical field can thus act as a lens for the electron beam. To achieve the chromatic correction it is necessary to generate the light lens with different tailored shapes for the different energy components within the electron beam. This can be accomplished by using a focused optical beam propagating against the electron beam (see Fig. 1(b)). Due to the pulsed electron beam, which has defined energy-time correlation (chirp), different energy components arrive to the site of interaction with the light field at different times. With proper setting of the synchronization of the electron and the optical pulse out of the optical beam focus, different energy components of the electron pulse experience different lensing strength (see Fig. 1(c)).

The ponderomotive chromatic aberration correction creates a linearly increasing convergent lens effect, where faster electrons experience stronger lensing than slower ones (see Fig. 1(c) top). Conversely, when using divergent lensing for chromatic correction, slower electrons should experience stronger lensing, which decreases linearly for faster electrons (see Fig. 1(c) bottom).

During the interaction with a laser field the electron

wave will acquire a ponderomotive phase shift, which is defined as [48, 53]:

$$\varphi(\mathbf{r}, t) = -(1/\hbar) \int_{-\infty}^{\infty} dt U(\mathbf{r}, t), \quad (2)$$

with the ponderomotive potential:

$$U(\mathbf{r}, t) = \frac{e^2}{2m_e\gamma} \left[ A_x^2(\mathbf{r}, t) + A_y^2(\mathbf{r}, t) + \frac{A_z^2(\mathbf{r}, t)}{\gamma^2} \right], \quad (3)$$

where  $\gamma = 1/\sqrt{1 - v_e^2/c^2}$  is the relativistic factor,  $v_e = c\sqrt{1 - 1/\left(1 + \frac{E}{E_{r0}}\right)^2}$  is the relativistic electron velocity in the  $z$  direction and  $\mathbf{A}(\mathbf{r}, t)$  is the vector potential. We consider a harmonic optical pulse traveling in the  $-z$  direction:

$$\varepsilon(\mathbf{r}, t) = \tilde{\mathbf{g}}(\mathbf{r}) \exp \left[ -\frac{(t - t_0 + \frac{z}{c})^2}{2\sigma_t^2} \right] e^{-i\omega(t + \frac{z}{c})}, \quad (4)$$

where  $\tilde{\mathbf{g}}(\mathbf{r})$  is the spatial profile of the laser field (see supplementary for details). The time envelope is described as a Gaussian pulse with  $t_0$  the time at the center of the pulse,  $\frac{z}{c}$  accounting for the propagation along the negative  $z$ -axis,  $\sigma_t$  the temporal duration of the pulse, and  $\omega$  the angular frequency. Considering that the envelopes vary slowly compared to the carrier frequency, we can use the simplification  $\mathbf{A}(\mathbf{r}, t) = \Re \left[ \frac{\varepsilon(\mathbf{r}, t)}{i\omega} \right]$  [48]. The pon-

deromotive phase is then:

$$\begin{aligned} \varphi(\mathbf{r}, t) = & -\frac{e^2}{2m_e\gamma\hbar\omega^2} \int dt \left[ |\tilde{g}_x|^2(\mathbf{r}) + |\tilde{g}_y|^2(\mathbf{r}) + \frac{1}{\gamma^2} |\tilde{g}_z|^2(\mathbf{r}) \right] \\ & \times \exp \left[ -\frac{(t - t_0 + \frac{z}{c})^2}{\sigma_t^2} \right] \sin^2 [\omega(t + z/c)]. \end{aligned} \quad (5)$$

When using a focused optical beam the ponderomotive phase  $\varphi(\mathbf{r}, t)$  has a gradient along the  $z$  axis. The coupling between the chirped electron pulse energy components  $E$  and the graded ponderomotive phase coordinate  $z$  occurs thanks to the electron pulse chirp and also the energy dependent velocity of the electrons. To calculate the ponderomotive phase in the rest frame of each energy component  $z'(E)$  we substitute for the laboratory frame coordinate  $z(E) = z'_0(E) + v_e t$ , where the first term models the longitudinal electron energy distribution due to the chirp  $z'_0(E) = (E - E_0)\tau_e v_0 / 2\Delta E$  and the second term  $v_e t$  accounts for the different velocities. In the linearized chirp model,  $\tau_e$  is the duration of the electron pulse and  $v_0$  is the electron velocity at  $E_0$ . Further, we can write  $\sin^2 [\omega(t + z/c)] = (1 - \cos[\omega(t + z/c)]/2)$  and neglect the integral over the cosine term due to the slowly varying envelope. Finally, the energy dependent ponderomotive phase is:

$$\begin{aligned} \varphi(x, y, E) \approx & -\frac{e^2}{4m_e\gamma\hbar\omega^2} \int dt \left[ |\tilde{g}_x|^2(x, y, E) + |\tilde{g}_y|^2(x, y, E) \right. \\ & \left. + \frac{1}{\gamma^2} |\tilde{g}_z|^2(x, y, E) \right] \\ & \times \exp \left[ -\frac{\left( t - t_0 + \frac{z'_0(E) + v_e t}{c} \right)^2}{\sigma_t^2} \right]. \end{aligned} \quad (6)$$

We further employ the Bluestein algorithm [59], to enable the propagation and shaping of an initial Gaussian optical field into the desired mode  $\tilde{\mathbf{g}}(\mathbf{r})$  used for the interaction with electrons (see supplementary material). This propagation method is faster than other propagation methods and is less sensitive to sampling, making it particularly suitable for this application. A successful aberration correction is achieved when the concavity of the sum of the aberration phase and the ponderomotive phase  $\chi_0(x, y, E) + \varphi(x, y, E)$  does not depend on the energy of the electrons  $E$ , making all of the energy components to focus at the same plane. This condition corresponds to minimizing  $\frac{\partial}{\partial E} \frac{\partial^2}{\partial \alpha^2} [\chi_0(x, y, E) + \varphi(x, y, E)]$ .

If we denote the initial wavefunction as  $\psi_0$  in the electron-light interaction plane, the intensity profile of the electron beam in the focal plane can be calculated as the incoherent sum of the contributions of the different

energies within the beam [57]:

$$\begin{aligned} I(x', y') = & \int_{-\infty}^{\infty} dE |\psi(x', y', E)|^2 \\ & \frac{1}{\sqrt{2\pi\sigma_E^2}} \times \exp \left[ -\frac{(E - E_0)^2}{2\sigma_E^2} \right], \end{aligned} \quad (7)$$

where  $\psi(x', y', E) = \mathcal{F}_{2D} (e^{i\chi(x, y, E)} e^{i\varphi(x, y, E)} \psi_0(x, y, E))$ ,  $\mathcal{F}_{2D}$  is the 2D Fourier transform and  $\sigma_E^2 = \Delta E^2 / (8 \ln 2)$  is the standard deviation squared of the energy distribution.

### III. RESULTS

The gradient in the optical field intensity, such as that produced by an unshaped Gaussian or vortex beam, inherently contributes to partial chromatic aberration correction of electron beams. However, we use here Zernike polynomials [60] (see supplementary material) to precisely tailor focusing and defocusing ponderomotive lenses, thus achieving superior chromatic aberration correction. We denote the modified laser beams further as vortex-like and Gaussian-like, referring, respectively, to the modified vortex and Gaussian beam. Despite the break in cylindrical symmetry occurring in tightly focused beams, for the rough optimization of the Zernike polynomial weights  $c_n^0$ , we can carry out the calculations and visualize the phases in 2D in the  $yE$ -plane, considering only the middle slice of the phase distribution.

The energy-dependent part of the aberration phase  $\chi_0$  at  $x = 0$  as a function of  $y$  and  $E$  is shown in Fig. 2(a). At low electron energies, of the order 1 keV, the contribution of chromatic aberration becomes dominant compared to other aberrations, significantly affecting the size of the electron probe and limiting its resolution [8]. As such, we model the electron beam with the chromatic aberration coefficient  $C_c = 8$  mm, central energy of  $E_0 = 1$  keV, FWHM energy spread  $\Delta E = 0.5$  eV, and a maximum electron convergence angle of  $\alpha_{\max} = 8$  mrad. The interaction with light is placed close to the electron cross-over, where the electron beam radius is  $w_e = 2$   $\mu\text{m}$ .

The chromatic aberration of the electron lens is corrected using either an optical vortex-like or a Gaussian-like beam, with a tailored phase and intensity profile, imprinted by an SLM positioned at the point where the optical beam is collimated. A Gaussian-like beam, with a central wavelength of  $\lambda_0 = 2060$  nm, a pulse duration of  $\tau_0 = 250$  fs, and focused using a numerical aperture (NA) of 0.14, requires approximately 4  $\mu\text{J}$  of pulse energy for chromatic correction. In comparison, a vortex-like beam demands about 16  $\mu\text{J}$  of pulse energy for the same application. The duration of the electron pulse is  $\tau_e = 1200$  fs and the central energy group velocity is  $v_0 = 0.06c$ . The temporal overlap of the electron pulse and the optical pulse envelopes is defined at the optical

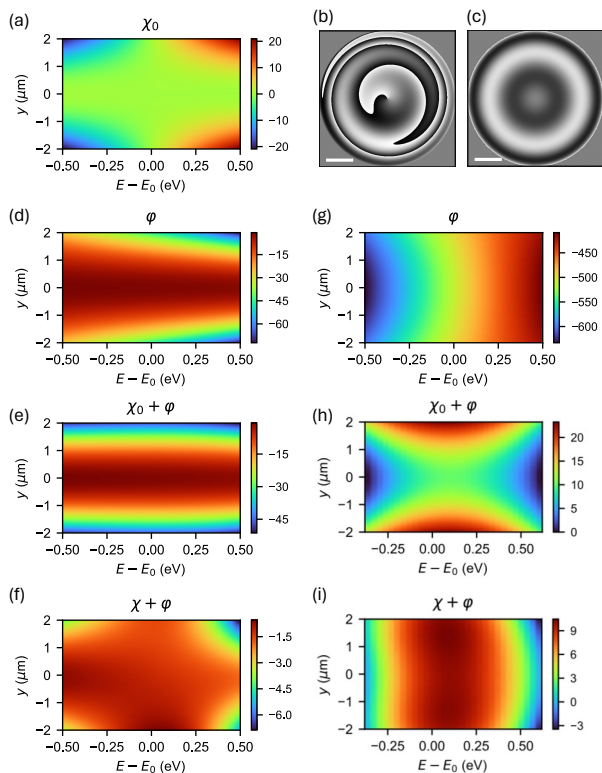


FIG. 2. Correction of chromatic aberration in traditional electron lenses and the compensation of ponderomotive phase shifts. The electron phase shifts, expressed in radians, are computed for each electron energy  $E$ . However, to enhance visualization, the x-axis displays  $E - E_0$  instead. (a) Energy-dependent chromatic aberration phase shift of the electron lens. The optical phase introduced by the spatial light modulator to the incident TEM<sub>00</sub> Gaussian mode leading to the (b) vortex beam (scale bar 1 cm, the phase varies from  $-\pi$  to  $\pi$ , white to black) and (c) Gaussian-like beam used to compensate color aberration. (d) Ponderomotive phase shift when using a shaped vortex laser beam. (e) Combined aberration phase and ponderomotive phase shift without and (f) with electron lens defocus. (g) Energy dependent ponderomotive phase shift when using a Gaussian-like beam. (h) Combined aberration phase and ponderomotive phase shift for a Gaussian-like beam without and (i) with electron lens defocus.

beam focus ( $z = 0$ ) when the coordinate systems of the electron and laser beams are aligned without spatial or temporal shifts. It is important to note that the exact temporal overlap also depends on the electron energy, as this influences the relative timing of the interaction. The shift in the optical beam focus relative to the temporal overlap is controlled by applying a lens phase to the optical fields. Figure 2(b) shows the Zernike-optimized phase profile applied to the incoming Gaussian beam to achieve the intensity distribution depicted in the top panel of Fig. 1(c), while Fig. 2(c) illustrates the phase profile used to produce the intensity distribution shown in the bottom panel of Fig. 1(c).

The vortex-like beam generates a ponderomotive phase shift, as shown in Fig. 2(d), which acts as a convergent lens. This effect causes stronger focusing on the higher-energy electrons, shifting their focal point backward. The final phase profile of the electron beam, which is given as  $\chi_0(x, y, E) + \varphi(x, y, E)$  has weaker energy dependence, as illustrated in Fig. 2(e). Adding an energy-independent positive defocus of  $\Delta z_0 = 8.5 \mu\text{m}$  can bring the focal point back to the geometrical focus of the  $E_0$  electron beam component, resulting in a nearly constant phase (see Fig. 2(f)). The slight asymmetry in Fig. 2(f) is caused by the finite resolution of the SLM resulting in the phase in Fig. 2(b), causing an effective axial misalignment of the focused optical beam.

The correction with a Gaussian-like mode is analogous, with the ponderomotive phase shift in Fig. 2(g) acting as an energy-dependent divergent lens in the energy difference region between -0.5 eV and 0.25 eV and pushing the less energetic components of the electron beam forward (see Fig. 2(h)). Then, as a result of the shaping, the ponderomotive potential curvature flips, and the ponderomotive phase acts as a convergent lens. Negative defocus of  $\Delta z_0 = -2.5 \mu\text{m}$  results in phase constant in the  $y$  direction (see Fig. 2(i)). In Figs. 2(h,i) we subtracted the  $y$ -independent component of the phase, which is linear in  $E$ . This component of the phase has no effect on the electron focal spot and only induces constant longitudinal acceleration, which can be neglected in this case. The linear phase change is  $\approx 200$  rad, which we estimate to yield an energy shift of  $\approx 0.12$  eV. Note that the acceleration can be tuned by shaping the longitudinal intensity profile of the laser beam, enabling advanced longitudinal wavefront shaping of electrons.

The electron beam focal spot with the chromatic aberration  $C_c = 8$  mm is shown in Fig. 3(a), and the ideal profile with zero  $C_c$  is shown in Fig. 3(b). In the goal profile there is a diffraction Airy ring due to the sharp aperture of the electron beam, however, in the aberrated beam focus profile, a large portion of the intensity is dispersed onto the background, leaving a weaker and wider central spot, with decrease to 1/4th. The characteristics may vary when the initial electron beam has a different transverse profile and energy distribution. The resulting electron profile after the ponderomotive phase shift is shown in Fig. 3(c) for a vortex-like beam and Fig. 3(d) for a Gaussian-like beam. We note that the intensity of the central peak after both corrections is over 80% of the target peak intensity compared to 25% in the aberrated beam intensity and that the energy dispersed in the background is significantly suppressed. Through correlation with beam focus profiles for various  $C_c$  we estimate that the effective  $C_{c,\text{eff}}$  achieved through correction is around 1.2 mm for the vortex-like beam and 1.1 mm for the Gaussian-like beam, resulting in improvement by a factor of 7 for these parameters.

Other criteria demonstrating chromatic correction include the reduction in the standard deviation of the electron probe profiles:  $\sigma_{\text{vortex}} = 2.67$  nm and  $\sigma_{\text{gauss}} =$

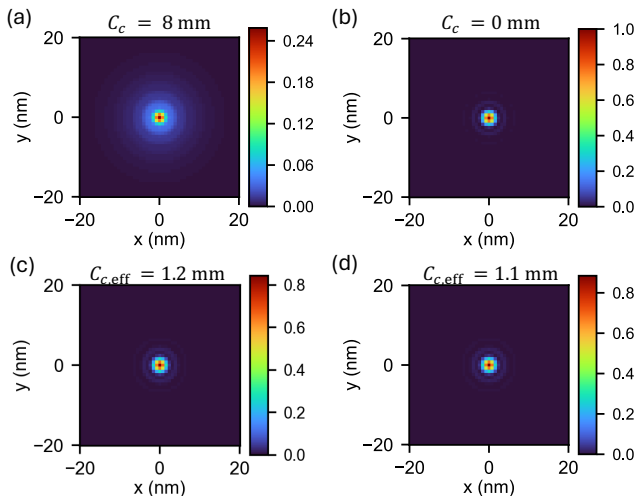


FIG. 3. (a) Electron focal spot with chromatic aberration coefficient  $C_c = 8$  mm. (b) Electron focal spot with chromatic aberration coefficient  $C_c = 0$  mm. (c) Electron focal spot after correction with a vortex beam. (d) Electron focal spot after correction with a Gaussian beam. The simulations are carried out using Eq. 7.

2.72 nm, compared to the aberrated beam  $\sigma_{\text{aber}} = 6.07$  nm and the target beam  $\sigma_{\text{goal}} = 2.39$  nm. Furthermore, there is a clear improvement in the contrast between the central peak and the background intensity.

#### IV. DISCUSSION AND CONCLUSION

Our study introduces a novel approach to mitigate chromatic aberrations in ultrafast electron microscopes using the ponderomotive potential generated by shaped optical fields. This method effectively compensates for chromatic distortions by tailoring the lensing strength to different energy components of a chirped electron beam. By creating a phase gradient along the longitudinal axis of the electron pulse, this strategy achieves energy-dependent ponderomotive lensing, reducing chromatic aberrations by approximately a factor of seven and significantly enhancing spatial resolution. In a Cc-uncorrected microscope, obtaining an equivalent focus spread (see Fig. 3 (d)) with a monochromator [2, 61, 62] would require narrowing the electron gun energy distribution by a factor of over 7 to  $\Delta E \sim 70$  meV. Note

that light-based chromatic correction techniques can be effective not only at low energies but also at higher electron energies, providing a pathway to improve resolution across a broader energy range.

The shaping of Gaussian and vortex beams using Zernike polynomials allowed for precise control over the light intensity distribution. This approach ensured a nearly linear variation in the axial direction and a quadratic dependence in the radial direction, optimizing the interaction with the electron pulse. In this study, phase-only shaping techniques were used and optimized using a modified gradient descent algorithm [63]. Incorporating also amplitude modulation alongside phase shaping could further enhance chromatic correction, potentially improving the overall performance and flexibility of the approach.

Despite its promise, certain limitations require attention. To minimize the induced ponderomotive phase shift distortions, it is recommended to use a laser with pulse energy stability better than 1% rms. Furthermore, improved beam-pointing stability can be achieved by integrating active piezo-driven beam-pointing stabilization systems, utilizing optical cavities [64], or spatial filtering.

For experimental validation, measuring electron defocus under varying electron energy distributions [8], the practical implementation of the method can be rigorously tested. More research is needed to explore the feasibility of simultaneously correcting chromatic and spherical aberrations using ponderomotive interactions.

In conclusion, ponderomotive interactions in free space offer a compelling solution to the challenge of chromatic aberrations in ultrafast electron microscopy.

#### ACKNOWLEDGMENTS

The authors acknowledge funding from the Czech Science Foundation (project 22-13001K), Charles University (SVV-2023-260720, PRIMUS/19/SCI/05, GAUK 90424) and the European Union (ERC, eWaveShaper, 101039339). Views and opinions expressed are however those of the author(s) only and do not necessarily reflect those of the European Union or the European Research Council Executive Agency. Neither the European Union nor the granting authority can be held responsible for them. This work was supported by TERA FIT project No. CZ.02.01.01/00/22\_008/0004594 funded by OP JAK, call Excellent Research.

[1] C. Weißbäcker and H. Rose, *Journal of electron microscopy* **50**, 383 (2001).  
 [2] U. Kaiser, J. Biskupek, J. C. Meyer, J. Leschner, L. Lechner, H. Rose, M. Stöger-Pollach, A. N. Khlobystov, P. Hartel, H. Mueller, *et al.*, *Ultramicroscopy* **111**, 1239 (2011).  
 [3] M. Linck, P. Hartel, S. Uhlemann, F. Kahl, H. Müller,

J. Zach, M. Haider, M. Niestadt, M. Bischoff, J. Biskupek, *et al.*, *Physical review letters* **117**, 076101 (2016).  
 [4] O. Scherzer, *Zeitschrift für Physik* **101**, 593 (1936).  
 [5] H. H. Rose, *Journal of electron microscopy* **58**, 77 (2009).  
 [6] O. Scherzer, *Optik* **2**, 114 (1947).  
 [7] J. Zach and M. Haider, *Nuclear Instruments and Methods in Physics Research Section A: Accelerators, Spec-*

- trometers, Detectors and Associated Equipment **363**, 316 (1995).
- [8] M. Haider, H. Rose, S. Uhlemann, E. Schwan, B. Kabius, and K. Urban, *Ultramicroscopy* **75**, 53 (1998).
- [9] A. H. Zewail, *science* **328**, 187 (2010).
- [10] Y. Morimoto and P. Baum, *Nature Physics* **14**, 252 (2018).
- [11] Y. Morimoto, *Microscopy* **72**, 2 (2023).
- [12] A. Feist, N. Bach, N. R. da Silva, T. Danz, M. Möller, K. E. Priebe, T. Domröse, J. G. Gatzmann, S. Rost, J. Schauss, *et al.*, *Ultramicroscopy* **176**, 63 (2017).
- [13] F. Houdellier, G. M. Caruso, S. Weber, M. Kociak, and A. Arbouet, *Ultramicroscopy* **186**, 128 (2018).
- [14] C. Zhu, D. Zheng, H. Wang, M. Zhang, Z. Li, S. Sun, P. Xu, H. Tian, Z. Li, H. Yang, *et al.*, *Ultramicroscopy* **209**, 112887 (2020).
- [15] C. Maurer, A. Jesacher, S. Bernet, and M. Ritsch-Marte, *Laser & Photonics Reviews* **5**, 81 (2011).
- [16] V. Grillo, E. Karimi, G. C. Gazzadi, S. Frabboni, M. R. Dennis, and R. W. Boyd, *Phys. Rev. X* **4**, 011013 (2014).
- [17] R. Shiloh, Y. Lereah, Y. Lilach, and A. Arie, *Ultramicroscopy* **144**, 26 (2014).
- [18] R. Shiloh, R. Remez, P.-H. Lu, L. Jin, Y. Lereah, A. H. Tavabi, R. E. Dunin-Borkowski, and A. Arie, *Ultramicroscopy* **189**, 46 (2018).
- [19] J. Verbeeck, A. Béch e, K. M uller-Caspary, G. Guzzinati, M. A. Luong, and M. Den Hertog, *Ultramicroscopy* **190**, 58 (2018).
- [20] F. V. Ib a nez, A. B ech e, and J. Verbeeck, “Can a programmable phase plate serve as an aberration corrector in the transmission electron microscope (tem)?” (2022).
- [21] D. Roitman, R. Shiloh, P.-H. Lu, R. E. Dunin-Borkowski, and A. Arie, *ACS photonics* **8**, 3394 (2021).
- [22] S. M. Ribet, S. E. Zeltmann, K. C. Bustillo, R. Dhall, P. Denes, A. M. Minor, R. Dos Reis, V. P. Dravid, and C. Ophus, *Microscopy and Microanalysis* **29**, 1950 (2023).
- [23] C.-P. Yu, F. Vega Ib a nez, A. B ech e, and J. Verbeeck, *SciPost Physics* **15**, 223 (2023).
- [24] B. Barwick, D. J. Flannigan, and A. H. Zewail, *Nature* **462**, 902 (2009).
- [25] A. Feist, K. E. Echternkamp, J. Schauss, S. V. Yalunin, S. Sch afer, and C. Ropers, *Nature* **521**, 200 (2015).
- [26] G. M. Vanacore, I. Madan, G. Berruto, K. Wang, E. Pomarico, R. Lamb, D. McGrouther, I. Kaminer, B. Barwick, F. J. Garc ıa de Abajo, *et al.*, *Nature communications* **9**, 2694 (2018).
- [27] G. M. Vanacore, G. Berruto, I. Madan, E. Pomarico, P. Biagioni, R. Lamb, D. McGrouther, O. Reinhardt, I. Kaminer, B. Barwick, *et al.*, *Nature materials* **18**, 573 (2019).
- [28] A. Kone cn a and F. J. G. de Abajo, *Physical Review Letters* **125**, 030801 (2020).
- [29] A. Ben Hayun, O. Reinhardt, J. Nemirovsky, A. Karnieli, N. Rivera, and I. Kaminer, *Science Advances* **7**, eabe4270 (2021).
- [30] R. Shiloh, J. Illmer, T. Chlouba, P. Yousefi, N. Sch onenberger, U. Niedermayer, A. Mittelbach, and P. Hommelhoff, *Nature* **597**, 498 (2021).
- [31] J.-W. Henke, A. S. Raja, A. Feist, G. Huang, G. Arend, Y. Yang, F. J. Kappert, R. N. Wang, M. M oller, J. Pan, *et al.*, *Nature* **600**, 653 (2021).
- [32] R. Dahan, A. Gorlach, U. Haeusler, A. Karnieli, O. Eyal, P. Yousefi, M. Segev, A. Arie, G. Eisenstein, P. Hommelhoff, *et al.*, *Science* **373**, eabj7128 (2021).
- [33] A. Feist, G. Huang, G. Arend, Y. Yang, J.-W. Henke, A. S. Raja, F. J. Kappert, R. N. Wang, H. Louren o-Martins, Z. Qiu, *et al.*, *Science* **377**, 777 (2022).
- [34] I. Madan, V. Leccese, A. Mazur, F. Barantani, T. LaGrange, A. Sapozhnik, P. M. Tengdin, S. Gargiulo, E. Rotunno, J.-C. Olaya, *et al.*, *ACS photonics* **9**, 3215 (2022).
- [35] S. Tsesses, R. Dahan, K. Wang, T. Bucher, K. Cohen, O. Reinhardt, G. Bartal, and I. Kaminer, *Nature Materials* **22**, 345 (2023).
- [36] F. J. Garc ıa de Abajo and C. Ropers, *Physical Review Letters* **130**, 246901 (2023).
- [37] J. H. Gaida, H. Louren o-Martins, S. V. Yalunin, A. Feist, M. Sivi, T. Hohage, F. J. Garc ıa de Abajo, and C. Ropers, *Nature Communications* **14**, 6545 (2023).
- [38] A. P. Synanidis, P. Gon alves, C. Ropers, and F. J. G. de Abajo, *Science Advances* **10**, eadp4096 (2024).
- [39] Y. Fang, J. Kuttruff, D. Nabben, and P. Baum, *Science* **385**, 183 (2024).
- [40] P. H. Bucksbaum, D. W. Schumacher, and M. Bashkansky, *Physical Review Letters* **61**, 1182 (1988).
- [41] D. L. Freimund, K. Afatooni, and H. Batelaan, *Nature* **413**, 142 (2001).
- [42] D. L. Freimund and H. Batelaan, *Physical review letters* **89**, 283602 (2002).
- [43] J. R. Dwyer, C. T. Hebeisen, R. Ernstorfer, M. Harb, V. B. Deyirmenjian, R. E. Jordan, and R. Dwayne Miller, *Philosophical Transactions of the Royal Society A: Mathematical, Physical and Engineering Sciences* **364**, 741 (2006).
- [44] P. Baum and A. H. Zewail, *Proceedings of the National Academy of Sciences* **104**, 18409 (2007).
- [45] M. Koz ak, N. Sch onenberger, and P. Hommelhoff, *Physical Review Letters* **120**, 103203 (2018).
- [46] O. Schwartz, J. J. Axelrod, S. L. Campbell, C. Turnbaugh, R. M. Glaeser, and H. M uller, *Nature methods* **16**, 1016 (2019).
- [47] J. J. Axelrod, S. L. Campbell, O. Schwartz, C. Turnbaugh, R. M. Glaeser, and H. M uller, *Physical review letters* **124**, 174801 (2020).
- [48] M. C. Chirita Mihaila, P. Weber, M. Schneller, L. Grandits, S. Nimmrichter, and T. Juffmann, *Physical Review X* **12**, 031043 (2022).
- [49] M. Tsarev, J. W. Thurner, and P. Baum, *Nature Physics* **19**, 1350 (2023).
- [50] S. Ebel and N. Talebi, *Communications Physics* **6**, 179 (2023).
- [51] B. Schaap, C. Sweers, P. Smorenburg, and O. Luiten, *Physical Review Accelerators and Beams* **26**, 074401 (2023).
- [52] C. I. Velasco and F. de Abajo, *arXiv preprint arXiv:2412.03410* (2024).
- [53] F. J. G. de Abajo and A. Kone cn a, *Physical Review Letters* **126**, 123901 (2021).
- [54] Y. Uesugi, Y. Kozawa, and S. Sato, *Physical Review Applied* **16**, L011002 (2021).
- [55] Y. Uesugi, Y. Kozawa, and S. Sato, *Journal of Optics* **24**, 054013 (2022).
- [56] M. C. C. Mihaila and M. Koz ak, *Opt. Express* **33**, 758 (2025).
- [57] M. Haider, S. Uhlemann, and J. Zach, *Ultramicroscopy* **81**, 163 (2000).
- [58] T. Kibble, *Physical Review* **150**, 1060 (1966).

- [59] Y. Hu, Z. Wang, X. Wang, S. Ji, C. Zhang, L. Jiawen, W. Zhu, D. Wu, and J. Chu, *Light Sci Appl* **9** (2020), [10.1038/s41377-020-00362-z](https://doi.org/10.1038/s41377-020-00362-z).
- [60] V. Lakshminarayanan and A. Fleck, *Journal of Modern Optics* **58**, 545 (2011).
- [61] K. Kimoto, *Journal of Electron Microscopy* **63**, 337 (2014).
- [62] N. L. Streshkova, P. Koutenský, T. Novotný, and M. Kozák, *Physical Review Letters* **133**, 213801 (2024).
- [63] G. Xie, Y. Ren, H. Huang, M. P. Lavery, N. Ahmed, Y. Yan, C. Bao, L. Li, Z. Zhao, Y. Cao, *et al.*, *Optics letters* **40**, 1197 (2015).
- [64] M. Peccianti, A. Pasquazi, Y. Park, B. E. Little, S. T. Chu, D. J. Moss, and R. Morandotti, *Nature communications* **3**, 765 (2012).